A CMOS-MEMS Mirror With Curled-Hinge Comb Drives

Huikai Xie, *Member, IEEE*, Yingtian Pan, and Gary K. Fedder, *Senior Member, IEEE*

***Abstract*—A micromirror achieves up to $\pm 4.7^\circ$ angular displacement with 18 Vdc by a comb-drive design that uses vertical angled offset of the comb fingers. Structures are made from a combination of CMOS interconnect layers and a thick underlying silicon layer. Electrical isolation of the silicon fingers is realized with a slight silicon undercut etch, which disconnects sufficiently narrow pieces of silicon under the CMOS microstructures. The 1 mm by 1 mm micromirror is made of an approximately 40 μm-thick single-crystal silicon plate coated with aluminum from the CMOS interconnect stack. The mirror has a peak-to-peak curling of 0.5 μm. Fabrication starts with a conventional CMOS process followed by dry-etch micromachining steps. There is no need for wafer bonding and accurate front-to-backside alignment. Such capability has potential applications in biomedical imaging, optical switches, optical scanners, interferometric systems, and vibratory gyroscopes.**

[975]

***Index Terms*—Curled-hinge comb drive, high-aspect-ratio, micromirror, out-of-plane actuation.**

I. Introduction

MICROMIRRORS have obtained extensive attention recently because of their applications in optical switches and displays. They are also used in a wide range of other applications, such as interferometric systems [1], optical spectroscopy [2], aberration correction [3] and biomedical imaging [4], [18]. The requirements of micromirrors vary with different applications. Flatness, roughness and reflectivity are the common metrics across most applications. For optical displays, fill factor and pixel size are the most important parameters. For optical switches, speed, maximum tilt angle and power consumption are primary requirements.

Micromirrors have been demonstrated by using different micromachining processes. A successful example of surface-micromachined micromirrors is Texas Instruments' digital mirror device (DMD) [5]. Scanning polysilicon micromirrors have also been used in barcode readers [6]. In order to overcome the small out-of-plane actuation range limited by the substrate electrode, vertical comb drives have been explored using various techniques to create uneven stationary and movable comb fingers. Selvakumar *et al.* employed a bulk/poly-silicon trench refill technology [7]. Yeh *et al.* reported a design with movable polysilicon comb fingers staggered above stationary bulk-Si comb fingers [8]. Syms demonstrated a 3-D microscanner using a surface-tension self-assembling technique [9]. All the mirrors mentioned above are made of thin-film materials. It is well known that it is difficult to achieve large flat thin-film mirrors with large tilt range due to the residual stress existing in thin-film structures. Bulk-micromachining processes have been used to make sidewall mirrors [10], but the sidewall angle, smoothness and area efficiency are concerns. Another choice is to combine surface- and bulk-micromachining processes. A single-crystal silicon (SCS) based micromirror was fabricated by using silicon-on-insulator (SOI) wafers and two-side alignment [11]. The stator and rotator comb fingers of the micromirror are at different height levels. An optical scanning angle of 24.9° was achieved with a 171 Vrms voltage at the resonant frequency (34 kHz) of the micromirror. Similar to the flip-chip thin-film micromirror array reported in [12], a 460 μm-by-460 μm SCS mirror was assembled on top of an electrostatic polysilicon actuator to achieve a flat surface [13]. The polysilicon actuator was 60 μm above the substrate, raised by self-assembled Micro-Elevator by Self-Assembly (MESA) structures [14]. The assembled SCS micromirror can perform two-dimensional (2-D) scanning with a maximum optical scanning angle of $\pm 7.5^\circ$. The same group reported a SCS micromirror with integrated angular comb drive actuation [15]. The tilt of the comb drives was realized by a hard-baked photoresist hinge, and the device was built on SOI wafers. Kwon *et al.* also demonstrated an SOI vertical comb actuator for moving microlenses [16].

The authors demonstrated a 1 mm by 1 mm, flat SCS micromirror that rotates 17° with thermal actuation at 12 mA current [17] and assembled the micromirror in an endocopic optical coherence tomography imaging system for the transverse laser scanning [18]. However, the large tilt angle at the rest position makes it difficult to align and perform symmetric scanning, and the scanning speed is limited by the thermal actuation.

The micromirror described in this paper is made of single-crystal silicon (SCS) and coated with aluminum [19]. A deep reactive-ion-etch (DRIE) CMOS-MEMS process [20], which is based on a previous thin-film CMOS-MEMS process [21], is employed. The micromachining process steps are performed after the foundry CMOS process steps are completed, and are completely compatible with conventional CMOS processes. Unlike the lateral comb drives, the stator

Manuscript received December 13, 2002; revised April 10, 2003. This work was supported in part by DARPA and the U.S. AFRL, under agreement F30602-99-2-0545, NIH Contract NIH-1-R01-DK059265-01, and the Whitaker Foundation Contract 00-0149. Subject Editor D. Cho.

H. Xie was with the Department of Electrical and Computer Engineering, Carnegie Mellon University, Pittsburgh, PA 15213 USA. He is now at the Department of Electrical and Computer Engineering, University of Florida, Gainesville, FL 32611 USA (e-mail: hkxie@ece.ufl.edu).

Y. Pan is with the Departments of Bioengineering, State University of New York at Stony Brook, Stony Brook, NY 11794 USA.

G. K. Fedder is with the Dept of Electrical & Computer Engineering and The Robotics Institute, Carnegie Mellon University, Pittsburgh, PA 15213 USA (e-mail: fedder@ece.cmu.edu).

Digital Object Identifier 10.1109/JMEMS.2003.815839

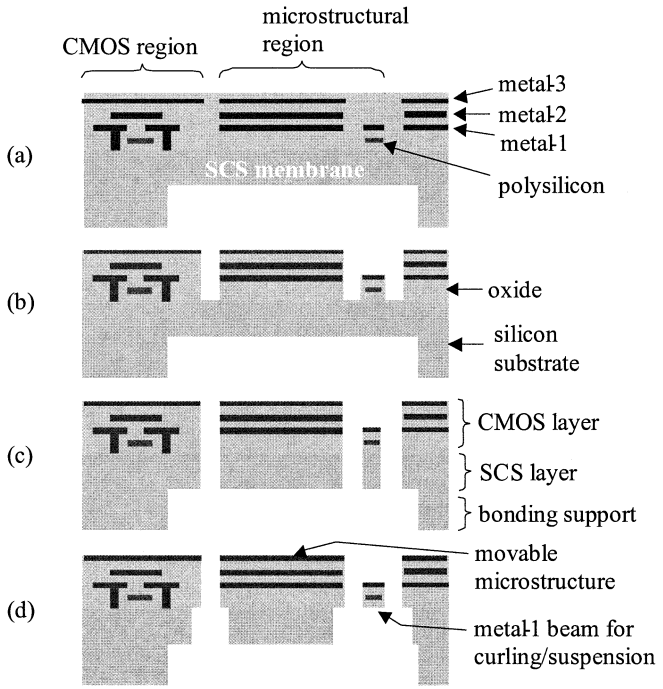

Fig. 1. DRIE CMOS-MEMS process flow: (a) backside etch; (b) oxide etch; (c) deep Si etch; and (d) Si undercut.

and rotor comb fingers of the z-axis comb drive do not lie in the same plane, and therefore large electrically actuated out-of-plane displacement is achieved. Though similar to the staggered comb drive reported in [11], this new design realizes the uneven stator and rotor comb fingers by using the curling of multilayer thin-film beams. Therefore, high-accuracy two-side alignment and expensive SOI wafers are not necessary.

II. DRIE CMOS-MEMS Process

It is well known that thin-film deposition processes generate residual stress and stress gradients, which cause curling. This curling limits the useful size of micromirrors. The small gap generated by the sacrificial layer present in surface-micromachined mirrors restricts their tilt range. In order to overcome the nonplanarity of thin-film CMOS microstructures, a thick bulk-silicon mirror is desirable. The present mirror introduces a single-crystal silicon (SCS) layer underneath CMOS multilayer structures in such a way that the mechanical properties are dominated by the SCS layer and electrical connections are provided by the CMOS interconnect metal layers. A backside etch is used to eliminate the remaining silicon substrate under the microstructures. Therefore, the microstructures can move vertically for hundreds of microns before encountering a limit stop.

The process flow is given in Fig. 1, and starts with the Agilent 3-metal 0.5 μm CMOS process. However, any CMOS process can be used. The backside silicon DRIE step leaves a 10 μm to 100 μm-thick SCS membrane [see Fig. 1(a)]. This step controls the thickness of the microstructure and forms a cavity ($\sim$ 250 μm deep) that allows the microstructure to move freely in a wide range. The depth of the cavity is determined by the thickness of the CMOS chips. Next, an anisotropic dielectric etch is performed from the frontside [see Fig. 1(b)], followed by DRIE

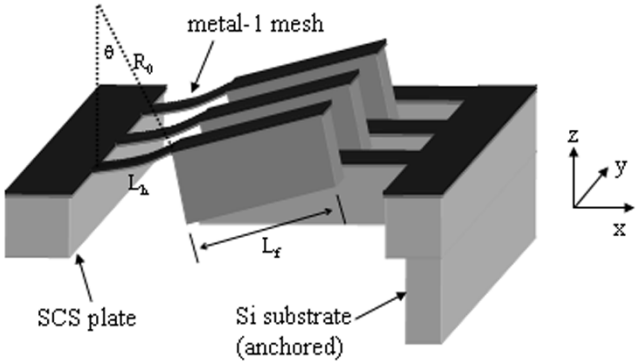

Fig. 2. Schematic of a curled-hinge comb drive.

of silicon [see Fig. 1(c)]. At the end of this step, a thick SCS layer remains underneath the CMOS layer, resulting in a flat released microstructure. Finally, a brief isotropic silicon etch is performed [see Fig. 1(d)]. Any beam with a half-width less than the silicon undercut will have no SCS layer underneath. This type of beam can be used to form electrically isolated SCS islands, purposefully curled-up structures or z-compliant springs.

III. Curled-Hinge Comb Drive

The metal-1 beam shown in Fig. 1(d) has only thin layers of interconnect aluminum and dielectrics. This beam curls up after it is released because the residual stress of the top aluminum is tensile and the residual stress of the underlying oxide is compressive. Judiciously placing and sizing the metal-1 beams that connect to the comb fingers creates a "curled-hinge" comb drive with the stationary and movable fingers at different levels. This concept of the curled-hinge comb drive is illustrated in Fig. 2. The comb drive has two parts: a set of tilted comb fingers and a set of level comb fingers. The tilted combs are composed of a curled metal-1 mesh as a hinge and an array of tilted fingers with a thick underlying SCS layer. The silicon substrate underneath the metal-1 mesh is completely undercut during the deep Si etch because the metal-1 mesh consists of only narrow beams. Therefore, the SCS chunks under the tilted comb fingers are electrically isolated from the silicon substrate. The SCS chunks then can be wired through CMOS contacts to any place on the chip, e.g., a bonding pad. When a voltage is applied to the comb drive, the tilted and level comb fingers will tend to align and thus an electrostatic rotational torque is generated. The initial angle of the tilted comb fingers depends on the length of the metal-1 mesh and can be 45° or even larger, so torque through a large rotation angle can be designed.

As shown in Fig. 2, the curling of the thin-film hinge lifts up the fingers on one side of the comb drive, allowing large out-of-plane actuation range. The out-of-plane angle of the tilted fingers depends on the hinge length. It was measured that the radius of curvature of metal-1 beams was about 280 μm for Agilent 0.5 μm 3-metal CMOS process by using a standard post-CMOS micromachining process [21]. Note that the plasma etch of oxide [see Fig. 1(b)] also removes 0.1–0.2 μm thick aluminum through ion milling. Metal-1 beams with different aluminum thicknesses will have different curvature. The thinner the aluminum layer, the smaller the radius of curvature of the

metal-1 beam. It is possible to intentionally increase the ion milling of the aluminum layer to obtain large curvature. Care must be taken not to damage vias.

As shown in Fig. 2, the fingers tilt along the tangential direction at the tip of the curled hinge. Therefore, $\theta = L/R_0$, where θ is the tilt angle, L is the hinge length and R_0 is the radius of curvature. Assume a 25° tilt angle and $R_0 = 280\ \mu\mathrm{m}$. Thus, $L = 122\ \mu\mathrm{m}$. The stiffness of the hinge also depends on the hinge width and thickness. The hinge is made of metal-1 beams which are 1.9 μm thick. The pitch of the curled-hinge fingers is about 15 μm. By considering the holes on the hinge for silicon undercut, the effective single hinge width is about 7.5 μm. The effective Young's Modulus of metal-1 beams is 69 GPa [26]. Therefore, the stiffness of a single hinge is given by $k_z = (Ewt^3/4L_h^3) = 2.0\ \mathrm{N/m}$, where E is the Young's modulus, w, t and L_h are the width, thickness and length of a single hinge, respectively. Since the thickness of the SCS layer is typically 40 μm and the finger length is approximately 150 μm, this portion of the fingers can be considered as rigid. Thus, the equivalent torsional stiffness with respect to the y-axis can be approximated as

$$k_{\phi y} = k_z \left(L_h + \frac{L_f}{2}\right)^2 = 7.6 \times 10^{-8}\ \mathrm{N \cdot m/rad/finger} \quad (1)$$

where L_f is the length of the SCS part of the finger. If only 5° tilt angle is needed, then $L_h = 24.4\ \mu\mathrm{m}$. Accordingly, k_z and $k_{\phi y}$ are 243 N/m and $2.4 \times 10^{-6}\ \mathrm{Nm/rad}$, respectively. $k_{\phi y}$ for 5° is about 30 times greater than that for 25°.

IV. Mirror Design

The curled-hinge comb drive in Fig. 2 shows the level comb fingers anchored on the substrate. Alternatively, the tilted comb fingers can be anchored. The top view of the micromirror design is illustrated schematically in Fig. 3(a), taking advantage of these two anchor options. The comb drives with anchors on the curled side are denoted as "$\mathbf{X}$" and those anchored on the level side are denoted as "$\mathbf{Y}$". The $\mathbf{X}$ comb drives pull the mirror up, and the $\mathbf{Y}$ comb drives pull the mirror down. The comb drives are distributed on two sides of the mirror to obtain bidirectional balanced rotation. The two sets of each comb drive double the y-axis torque and zero the net z-axis force. The comb drives $\mathbf{X}1/\mathbf{Y}1$ rotate the mirror clockwise, and $\mathbf{X}2/\mathbf{Y}2$ rotate the mirror counterclockwise, as shown in Fig. 3(b) and (c).

V. Torsional Spring Design

A torsional beam is simple and robust as a suspension, but the utilization of chip area is poor. If a folded beam flexure is used, the z-axis compliance as well as the out-of-plane compliance is obtained. It has been found that a curled, folded beam flexure increases the resonant frequency of the z-axis mode, ω_z, by a factor of 3 [22]. Thermomechanical FEM simulation [23] also shows that the microstructure reported in [22] lowers ω_θ/ω_z from 1.3 for flat spring beams to 0.4 for curled spring beams, where ω_θ is the resonance frequency of the torsional mode. Therefore, a curled, folded spring design is employed to realize torsional compliance, as shown in Fig. 4. The vertical

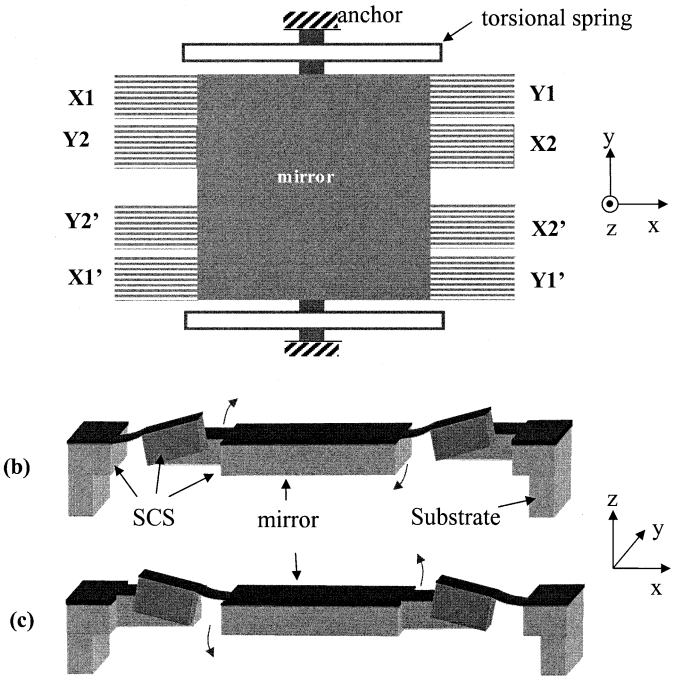

Fig. 3. Topology of the micromirror design. The combs labeled X1, X1′, X2 and X2′ have their curled-hinge comb fingers anchored, and therefore pull up on the mirror. The combs labeled Y1, Y1′, Y2 and Y2′ have their level comb fingers anchored, and therefore pull down on the mirror.

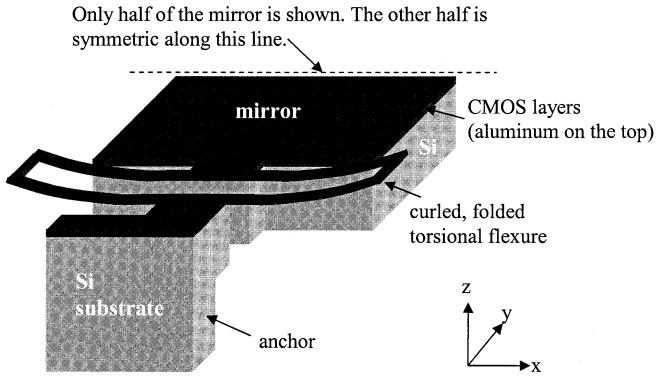

Fig. 4. Schematic of a folded torsional spring.

curling of the spring beams is generated by using the same technique as that for the curled-hinge comb drive discussed above. Regarding the analytical analysis of spring constants of folded mechanical flexures, interested readers may refer to [25].

One of the design concerns is that the stiffness of the comb drive hinge should be much greater than that of the torsional spring of the mirror plate. The mirror plate can be considered as a thin sheet since its lateral dimensions are much larger than its thickness. Therefore, the moment of inertia of the mirror plate along the y-axis is given by

$$I_{y,m} = \frac{MW_m^2}{12} = \rho(L_m W_m t_m)\frac{W_m^2}{12} \quad (2)$$

where M, ρ, W_m, L_m and t_m are respectively the mass, mass density, width, length and thickness of the mirror plate. Since the majority of the mirror plate is silicon, ρ can be approximated as the mass density of silicon which is 2700 $\mathrm{kg/m^3}$.

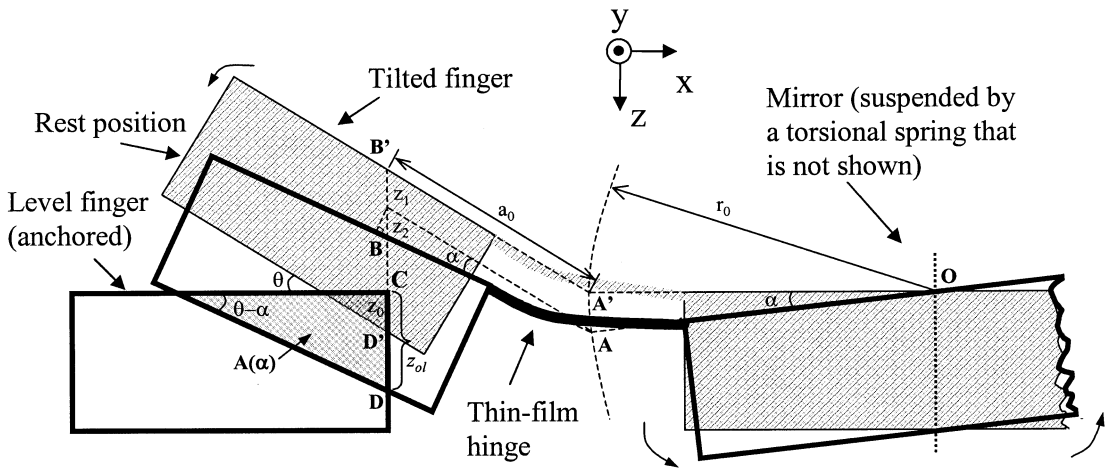

Fig. 5. Cross section of the curled-hinge comb drive for rotation analysis. **O** is the rotation center, **A** is the intersection of the extended lines of the tilted finger top and the mirror surface, **B** is the intersection of the tilted finger top with the extended line of the level finger edge and C is the upper-right corner of the level finger.

Using (2), for a mirror plate 1 mm by 1 mm by 40 μm thick, $I_{y,m} = 9.0 \times 10^{-15}$ kg $\cdot$ m^2. Thus, if a torsional resonant frequency of 200 Hz is desired, the required spring constant of the torsional spring should be equal to $k_{\phi y,m} = I_{y,m}(2\pi \cdot 200)^2 = 1.4 \times 10^{-8}$ N $\cdot$ m/rad, which is less than one fifth of the torsional spring constant of a single hinge of the comb drives with 25° initial tilt angle [see (1)]. Typically, each group of the comb drives has about 20 curled-hinge fingers. So, the hinges of the comb drives are about two orders of magnitude stiffer than the torsional spring, implying that the torsional spring could be one order of magnitude stiffer, or the resonant frequency of the mirror could be improved to 650 Hz.

If even higher speed is needed, reducing the initial angle from 25° to 5° will increase the hinge stiffness by a factor of 30, as discussed in the previous section. The number of curled-hinge fingers can also be increased by a factor of 2 to 5. Therefore, 5 kHz to 10 kHz resonant frequency is achievable. Further increasing speed is still possible, but at the price of reducing mirror size or increasing chip size.

VI. Electrostatic Force Analysis

Fig. 5 shows the cross section of a curled-hinge comb drive. The finger of the comb drive with curled metal-1 hinge tilts out-of-plane with an angle, θ, at the rest position. According to the rough analysis in the previous section, it is reasonable to assume that the assembly of the tilted finger, the curved thin-film connection and the mirror is rigid with respect to the torsional spring flexure. Thus, the whole assembly rotates at the same angle, α.

In order to estimate the performance of the curled comb drive, the electrostatic force must be first calculated. The electrostatic force in the z-direction is given by

$$F_z = \frac{N}{2} \cdot \frac{dC}{dz} \cdot V^2 = \frac{N}{2} \cdot \frac{1}{l \cdot \cos\alpha} \cdot \frac{dC}{d\alpha} \cdot V^2 \tag{3}$$

where C is the sidewall capacitance per comb finger, N is the number of comb fingers, V is the applied voltage and l is the distance from the force source to the rotation center, O. The torque associated with the force and the torsional stiffness, k_ϕ, of the folded flexure determine the rotation angle

$$\alpha = \frac{F_z \cdot l \cdot \cos\alpha}{k_\phi} = \frac{N \cdot V^2}{2\omega_r^2 I} \frac{dC}{d\alpha} \tag{4}$$

where $\omega_r = \sqrt{k_\phi / I}$, is the resonance frequency and $I = (1/12)\rho \cdot h \cdot l \cdot w^3$, is the moment of inertia of the mirror plate. For sizing purposes during design, a parallel-plate approximation is used to estimate capacitance

$$C(\alpha) = \frac{\varepsilon_0 A(\alpha)}{g} \tag{5}$$

where ε_0 is the vacuum permittivity $(8.854 \times 10^{-12}$ F/m), g is the comb finger gap, and $A(\alpha)$ is the overlap area between the level and tilted fingers. When calculating $A(\alpha)$, sections of the right edge of the level finger and its extension line are used, as shown in Fig. 5. Note that $\boldsymbol{BB'} = \boldsymbol{DD'} + \boldsymbol{\Delta z}$, where $\Delta z = \boldsymbol{h}((1/\mathbf{cos}(\theta)) - (1/\mathbf{cos}(\theta - \alpha)))$. There are three cases when calculating the overlap area.

1) When α is small, the tilted finger completely covers the upper-right corner of the level finger but does not exceed the lower-right corner of the level finger. In this case, the overlap area is given by

$$\begin{aligned} \boldsymbol{A}(\alpha) &= \frac{1}{2}\frac{1}{\tan(\theta - \alpha)} z_{ol}^2 \\ &= \frac{1}{2}\frac{1}{\tan(\theta - \alpha)} (z_0 + z_1 + z_2 - \Delta z)^2 \end{aligned} \tag{6}$$

where $z_{ol} = z_0 + z_1 + z_2 - \boldsymbol{\Delta z}$ is the overlap at the right edge of the level finger, z_0 is the overlap at the rest position, and z_1 plus z_2 is the z-axis displacement at the edge. z_0, z_1 and z_2 are given by

$$z_0 = \frac{h}{\cos\theta} - a_0 \sin\theta, \tag{7}$$

$$z_1 = 2r_0 \sin\left(\frac{\alpha}{2}\right)\left(\cos\left(\frac{\alpha}{2}\right) - \tan\theta \sin\left(\frac{\alpha}{2}\right)\right) \tag{8}$$

$$z_2 = \frac{a_0 \sin\alpha}{\cos(\theta - \alpha)} \tag{9}$$

where h is the thickness of the comb fingers, r_0 is the distance from point O to point A, and a_0 is the distance from point A to point B.

TABLE I
DESIGN PARAMETER VALUES OF THE CURLED-HINGE COMB FINGER (SEE FIG. 5)

l	W	h	ρ	g	N
1 mm	1 mm	50 μm	2330 kg/m^3	3 μm	120
k_ϕ	ω_r	θ	a_0	r_0	
22 nN·m/rad	240 Hz	15°	160 μm	1 mm	

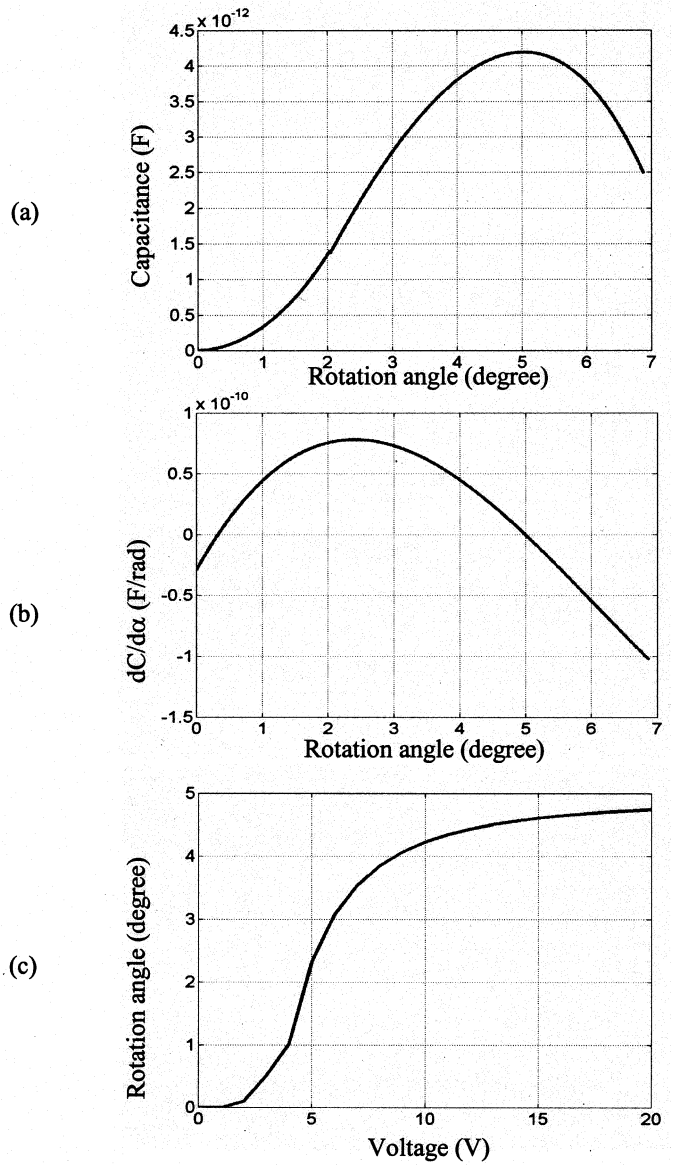

Fig. 6. Rotation analysis of the curled-hinge comb drive. (a) Capacitance versue angle. (b) Capacitance gradient with respect to angle. (c) Rotation angle versus applied voltage.

2) When α becomes larger, the tilted finger exceeds the lower-right corner, i.e., $z_{ol} > h$, but still covers the upper-right corner of the level finger. The total overlap area is subtracted by the exceeded area and is given by

$$A(\alpha) = \frac{1}{2} \cdot \frac{1}{\tan(\theta - \alpha)} \left[z_{ol}^2 - (z_{ol} - h)^2 \right]. \quad (10)$$

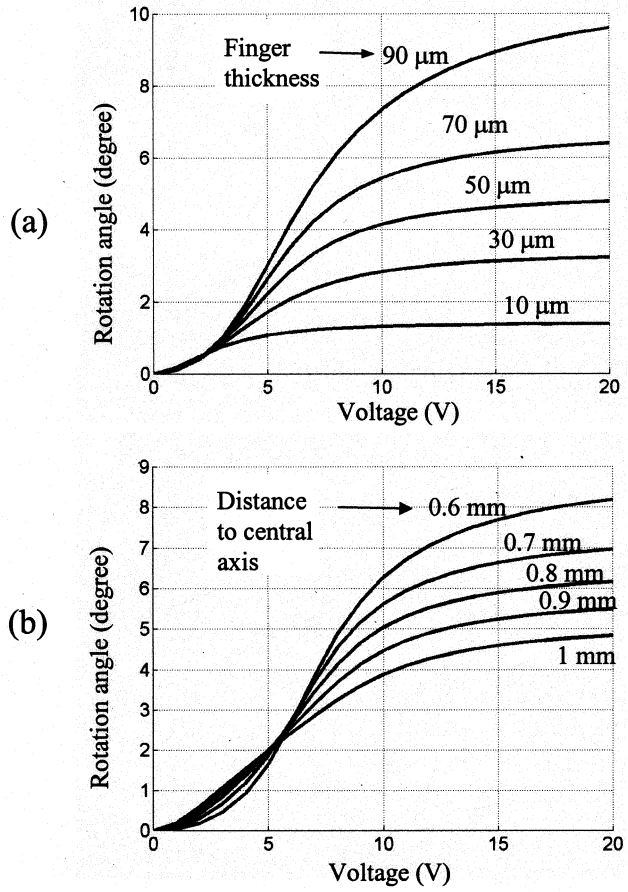

Fig. 7. Rotation angle dependence on geometric parameters. (a) Thickness of the comb fingers. (b) Distance from the comb drives to the central rotational axis.

3) When α becomes even larger, the upper-right corner of the level finger will be exposed, i.e., $\alpha > \alpha_0$, where α_0 is the angle when $\mathrm{BC} = 0$. α_0 is obtained by numerically solving the following equation:

$$a_0 \sin\theta - (z_1 + z_2) = 0. \quad (11)$$

In this case, the total overlap area must also exclude the exposed area and is given by

$$A(\alpha) = \frac{1}{2} \cdot \frac{1}{\tan(\theta - \alpha)} \times \left[z_{ol}^2 - (z_{ol} - h)^2 - (z_1 + z_2 - a_0 \sin\theta)^2 \right]. \quad (12)$$

The parameter values for the designed mirror are listed in Table I. Evaluating (5)to (12), $C(\alpha)$ and $dC/d\alpha$ are obtained as plotted in Fig. 6(a) and (b). The capacitance reaches its maximum value at a rotation angle of 5°. Substituting $dC/d\alpha$ into (4) and solving the torque balance equation, i.e.,

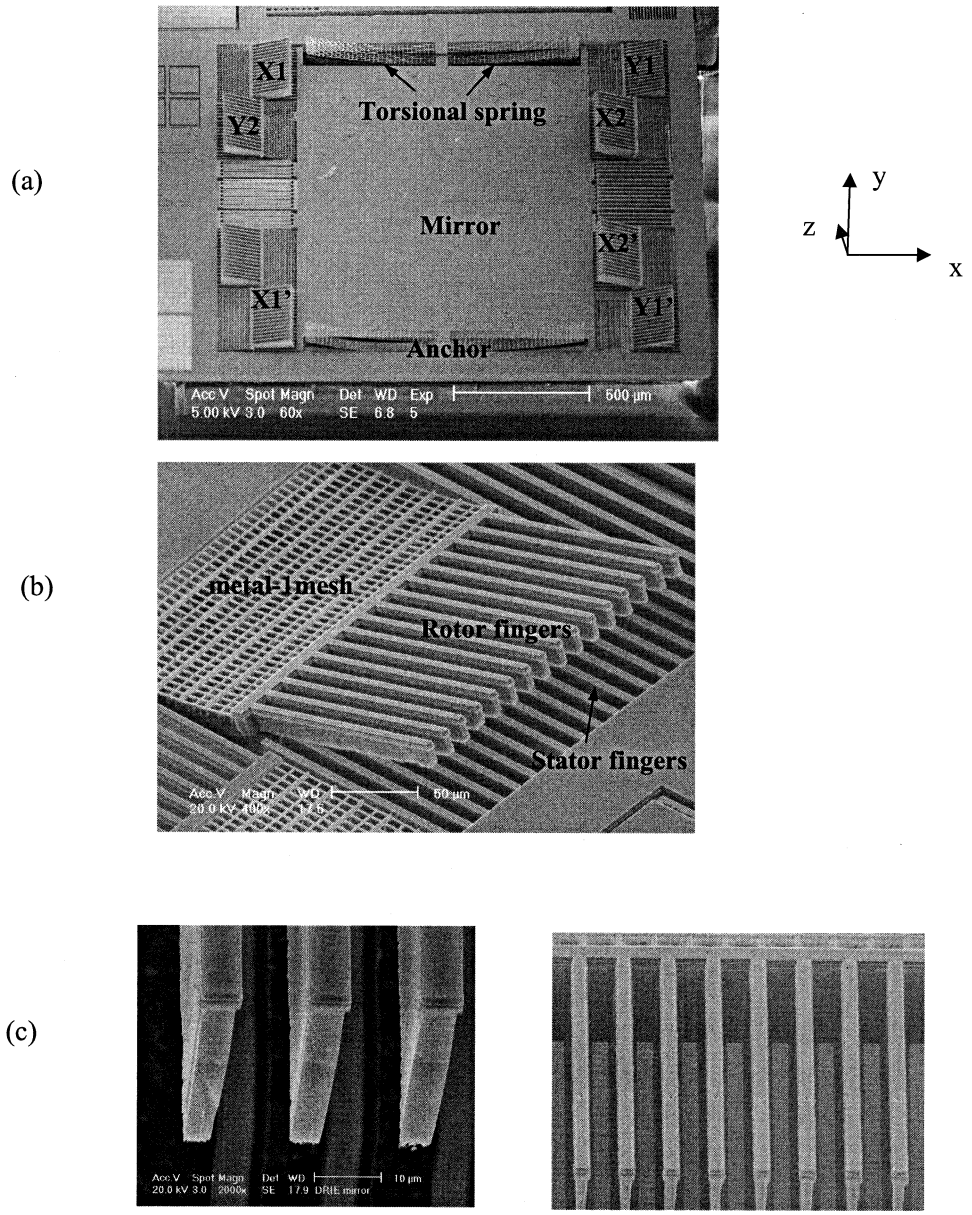

Fig. 8. SEMs of the micromirror with curled-hinge comb drives. (a) Top view of a released electrostatic micromirror. (b) Curled-hinge comb drive. (c) Close-up of tilted comb fingers.

$\tau_{\text{spring}}(\alpha) = \tau_{es}(\alpha, V)$, gives the static relationship between the rotation angle and applied voltage, as shown in Fig. 6(c). It is clear that the rotation of the mirror changes rapidly around 5 V and then saturates at about 4.8°.

Rotation angle dependencies on the finger thickness and the distance of the comb drive to the rotational axis are plotted in Fig. 7. As shown in Fig. 7(a), the rotation angle is very sensitive to finger thickness. The maximum rotation angle is doubled as the finger thickness increases from 50 μm to 90 μm. Placing comb drives closer to the rotational axis also significantly increases the maximum rotation angle without increasing drive voltage, as shown in Fig. 7(b).

VII. Experimental Results

The top view of a released 1 mm by 1 mm micromirror is shown in Fig. 8(a). A view of a curled-hinge comb is shown in Fig. 8(b). The lengths of the metal-1 mesh and the SCS fingers are 120 μm and 150 μm, respectively. The thickness of the SCS chunks is about 40 μm. Fig. 8(c) is a close-up of the comb fingers. An initial undercut of about 0.2 μm is used to assure the complete undercut of silicon underneath the metal-1 meshes and z-compliant springs. To further guarantee the electrical isolation of the silicon chunks, an n-doped well (with p-substrate) is placed underneath the metal-1 meshes and z-compliant springs. All of the tested devices had electrically isolated combs.

The profile of the mirror surface was characterized by using a Wyko NT2000 3D optical profiler. The measured peak-to-peak curling across the entire mirror is 0.5 μm (see Fig. 9). Simply increasing the thickness of the SCS layer will reduce curling. Alternatively, stress in custom thin-film layers may be tuned to increase flatness. For instance, it was found that metal-1 beams with field oxide removed and just gate oxide left are much flatter than those with field oxide underneath [26].

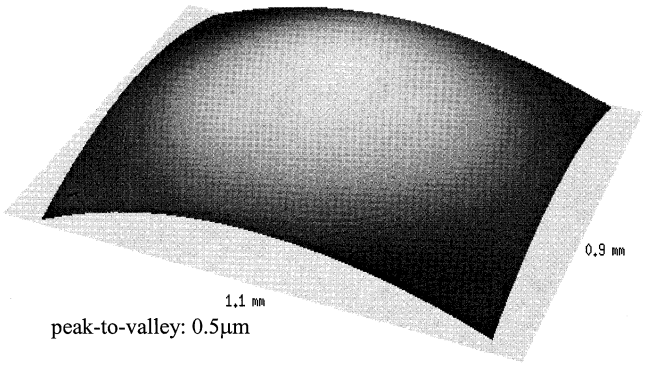

Fig. 9. Contour plot of the mirror profile measured with an optical profiler.

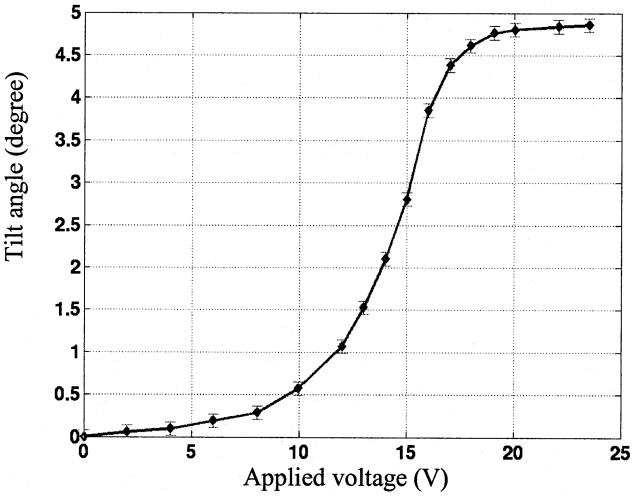

Fig. 10. The mirror rotation angle versus applied voltage.

Fig. 10 shows the measured rotation angle versus the applied voltage. Applying 18 V results in a tilt of 4.7°. Since the width of the entire device is 1.5 mm, the z-displacement at the comb-finger tips is 62 μm. The center plate can rotate to both sides and therefore a total rotation angle of 9.4° can be achieved. The rotation angle saturates above 20 V. The measured saturation angle is in good agreement with the analysis result plotted in Fig. 6(c). However, the measured voltage corresponding to the rapid rotation angle change is 15 V, instead of 5 V in the analysis. This is because the analysis assumed straight sidewalls for all the comb fingers. In reality, the cross section of the comb fingers consists of a wider metal/oxide layer on the top of a narrower but much thicker SCS layer. The fringing effects and the slope of the SCS sidewalls will change the capacitance gradient, which is not included in the simplified model shown in Fig. 5.

The frequency response measured by using an optical microvision system [24] is plotted in Fig. 11. The torsional resonant frequency is 233 Hz at very low applied drive voltage. The resonance frequency of this type of micromirrors can be increased to 10 kHz range, if needed, by increasing the spring stiffness and drive voltage. Of course, the stiffness of the hinges should be also increased accordingly, and the mirror size may have to be reduced, as discussed in a previous section. For high-resonance micromirrors, operating at the resonance frequency may be required to achieve desired scanning range.

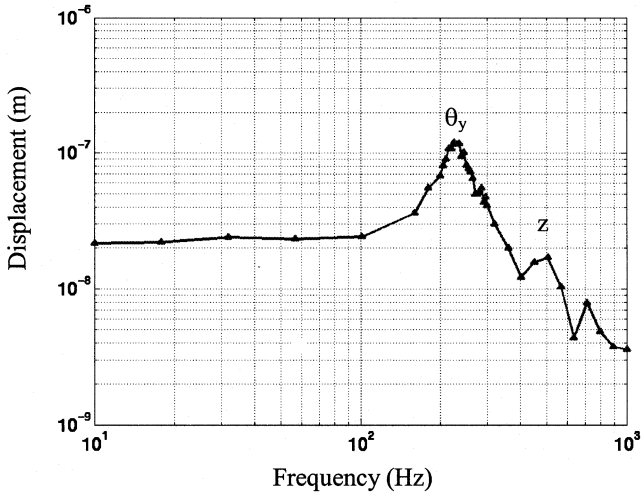

Fig. 11. Frequency response measured by using an optical microvision system.

VIII. Conclusion

A large, flat micromirror with large out-of-plane actuation has been experimentally demonstrated. The 9.4° rotation angle of the 1 mm by 1 mm mirror is limited by the implemented comb design. The mirror topology can be optimized for larger rotation angle or larger size. For example, by simply moving the curled-hinge comb drives from the two sides of the mirror closer to the central axis of the mirror, much larger rotation angle will be achieved. The mirror has adequate tilt angle and bandwidth for potential application in certain optical switches, optical scanners and medical imaging.

References

[1] F. A. Chollet, G. M. Hegde, A. K. Asundi, and A.Aiqun Liu, "Simple extrashort external-cavity laser self-mixing interferometer for acceleration sensing," in *Proc. SPIE—The Int. Society for Optical Engineering*, vol. 4596, 2001, pp. 272–279.

[2] K. J. Kearney and Z. Ninkov, "Characterization of a digital micromirror device for use as an optical mask in imaging and spectroscopy," in *Proc. SPIE—The Int. Society for Optical Engineering*, vol. 3292, 1998, pp. 81–92.

[3] P. Himiner and D. Dickensheets, "High speed, large deflection deformable mirrors for focus and spherical aberration control," in *Proc. 2002 IEEE/LEOS Int. Conference on Optical MEMS (Cat. no. 02EX610)*, 2002, pp. 193–194.

[4] U. Hofmann, S. Muehlmann, M. Witt, K. Dorschel, R. Schutz, and B. Wagner, "Electrostatically driven micromirrors for a miniaturized confocal laser scanning microscope," in *Proc. SPIE—The International Society for Optical Engineering*, vol. 3878, 1999, pp. 29–38.

[5] L. J. Hornbeck, "Current status of the digital micromirror device (DMD) for projection television applications," in *Tech. Dig. International Electron Devices Meeting*, Washington, DC, 1993, pp. 381–384.

[6] M.-H.Meng-Hsiung Kiang, O. Solgaard, R. S. Muller, and K. Y. Lau, "Micromachined polysilicon microscanners for barcode readers," *IEEE Photon. Technol. Lett.*, vol. 8, no. 12, pp. 1707–1709, Dec. 1996.

[7] A. Selvakumar, K. Najafi, W. H. Juan, and S. Pang, "Vertical comb array microactuators," in *Proc. IEEE Micro Electro Mechanical Systems, 1995, MEMS '95*, 29 Jan.–2 Feb. 1995, pp. 43–48.

[8] J.-L. A. Yeh, H.Hongrui Jiang, and N. C. Tien, "Integrated polysilicon and DRIE bulk silicon micromachining for an electrostatic torsional actuator," *J. Microelectromech. Syst.*, vol. 8, pp. 456–465, Dec. 1999.

[9] R. R. A. Syms, "Surface tension powered self-assembly of 3-D micro-optomechanical structures," *J. Microelectromech. Syst.*, vol. 8, pp. 448–455, Dec. 1999.

[10] W.-H. Juan and S. W. Pang, "High-aspect-ratio Si vertical micromirror arrays for optical switching," *J. Microelectromech. Syst.*, vol. 7, pp. 207–213, 1998.

[11] R. Conant, J. Nee, K. Lau, and R. S. Muller, "A flat high-frequency scanning micromirror," in *Tech.Dig. 2000 Solid-State Sensor & Actuator Workshop*, Hilton Head Island, SC, June 4–8, 2000, pp. 6–9.
[12] A. Tuantranont, V. M. Bright, L. A. Liew, W. Zhang, and Y. C. Lee, "Smart phase-only micromirror array fabricated by standard CMOS process," in *Proc. IEEE MEMS 2000*, Miyazaki, Japan, Jan. 25–28, 2000, pp. 455–460.
[13] G.-D. Su, H. Toshiyoshi, and M. C. Wu, "Surface-micromachined 2-D optical scanners with high-performance single-crystalline silicon micromirrors," *IEEE Photon. Technol. Lett.*, vol. 13, pp. 606–608, 2001.
[14] L. Fan, M. Wu, K. Choquette, and M. Crawford, "Self-assembled microactuated XYZ stages for optical scanning and alignment," in *Proc. Int. Solid State Sensors and Actuators Conf. (Transducer '97)*, Chicago, IL, pp. 319–322.
[15] P. R. Patterson, D.Dooyoung Hah, H.Hung Nguyen, H.H. Toshiyoshi, R.-M.Ru-Min Chao, and M. C. Wu, "A scanning micromirror with angular comb drive actuation," in *Proc. The Fifteenth IEEE International Conference on Micro Electro Mechanical Systems—MEMS'02*, Las Vegas, Nevada, Jan. 20–24, 2002, pp. 544–547.
[16] S. Kwon, V. Milanovic, and L. P. LEE, "Large-displacement vertical microlens scanner with low driving voltage," *IEEE Photon. Technol. Lett.*, vol. 14, pp. 1572–1574, 2002.
[17] H. Xie, Y. Pan, and G. K. Fedder, "A SCS CMOS micromirror for optical coherence tomographic imaging," in *Proc. IEEE MEMS 2002*, Las Vegas, Nevada, USA, Jan. 20–24, 2002, pp. 495–499.
[18] Y. Pan, H. Xie, and G. K. Fedder, "Endoscopic optical coherence tomography based on a CMOS-MEMS micromirror," *Opt. Lett.*, vol. 26, pp. 1966–1968, 2001.
[19] H. Xie, Y. Pan, and G. K. Fedder, "A CMOS-MEMS micromirror with large out-of-plane actuation," in *Proc. 2001 ASME International Mechanical Engineering Congress and Exposition—IMECE'01*, New York, Nov. 11–16, 2001.
[20] H. Xie, L. Erdmann, X. Zhu, K. Gabriel, and G. K. Fedder, "Post-CMOS processing for high-aspect-ratio integrated silicon microstructures," *J. Microelectromech. Syst.*, vol. 11, pp. 93–101, 2002.
[21] G. K. Fedder, S. Santhanam, M. Reed, S. Eagle, D. Guillou, M. Lu, and L. R. Carley, "Laminated high-aspect-ratio microstructures in a conventional CMOS process," *Sens. Actuators, Phys. A*, vol. A57, pp. 103–110, 1996.
[22] H. Xie and G. K. Fedder, "A CMOS-MEMS lateral-axis gyroscope," in *Tech. Dig. 14th IEEE International Conference on Micro Electro Mechanical Systems (MEMS 2001)*, Interlaken, Switzerland, Jan. 21–25, 2001, pp. 162–165.
[23] MEMCAD User's Manual. Coventor, Inc., Cary, NC 27513. [Online]http://www.coventor.com
[24] W. Hemmert, M. Mermelstein, and D. Freeman, "Nanometer resolution of 3-D motions using video interference microscopy," in *Tech. Dig. 12th IEEE International Conference on Micro Electro Mechanical Systems (MEMS'99)*, Orlando, FL, Jan. 19–23, 1999, pp. 302–308.
[25] G. K. Fedder, "Simulation of microelectromechanical systems," Ph.D. dissertation, University of California-Berkeley, 1994.
[26] M. Lu, X. Zhu, and G. K. Fedder, "Mechanical property measurement of 0.5-μm CMOS microstructures," in *Proc. Materials Research Society 1998 Spring Meeting*, San Francisco, CA, Apr. 13–17, 1998, pp. 27–32.

Huikai Xie (M'00) received the M.S. degree in electrooptics from Tufts University, Medford, MA, in 1998 and the Ph.D. degree in electrical and computer engineering from Carnegie Mellon University, Pittsburgh, PA, in 2002. He also received the B.S. and M.S. degrees in electronic engineering from Beijing Institute of Technology, China.

From 1992 to 1996, he was a research faculty member in the Institute of Microelectronics at Tsinghua University, Beijing, working on various silicon-based chemical and mechanical sensors. He is an Assistant Professor at the Department of Electrical and Computer Engineering of the University of Florida, Gainesville. He spent summer 2001 at the North America Research Center of Robert Bosch Corporation designing a 6-DOF inertial measurement unit. He has over 30 technical papers. His present research interests include integrated microsensors, optical MEMS, optical switching, biomedical imaging and sensing, and fiber-optic sensors.

Yingtian Pan is Assistant Professor of Biomedical Engineering at SUNY Stony Brook. His current research is focused on biomedical imaging and bioinstrumentation. He has over 30 journal publications in the related fields.

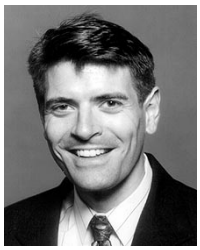

Gary K. Fedder (S'93–M'95–SM'01) received the B.S. and M.S. degrees in electrical engineering from the Massachusetts Institute of Technology (MIT), Cambridge, in 1982 and 1984, respectively. In 1994, he received the Ph.D. degree from University of California at Berkeley, where his research resulted in the first demonstration of multimode control of a underdamped surface-micromachined inertial device.

From 1984 to 1989, he worked at the Hewlett-Packard Company on circuit design and printed-circuit modeling. He is a Professor at Carnegie Mellon University holding a joint appointment with the Department of Electrical and Computer Engineering and The Robotics Institute. He has contributed to over 90 research publications and several patents in the MEMS area. His research interests include microsensor and microactuator design and modeling, integrated MEMS manufactured in CMOS processes and structured design methodologies for MEMS.

Dr. Fedder received the 1993 AIME Electronic Materials Society Ross Tucker Award, the 1996 Carnegie Institute of Technology G.T. Ladd Award, and the 1996 NSF CAREER Award. Currently, he serves as a subject editor for the IEEE/ASME JOURNAL OF MICROELECTROMECHANICAL SYSTEMS, on the editorial board of the IoP *Journal of Micromechanics and Microengineering* and as co-editor of the Wiley-VCH Sensors Update book series.